A New Bruker IFS 125HR FTIR Spectrometer for the Polar Environment Atmospheric Research Laboratory at Eureka, Nunavut, Canada: Measurements and Comparison with the Existing Bomem DA8 Spectrometer

REBECCA L. BATCHELOR, KIMBERLY STRONG, AND RODICA LINDENMAIER

Department of Physics, University of Toronto, Toronto, Ontario, Canada

RICHARD L. MITTERMEIER AND HANS FAST

Environment Canada, Toronto, Ontario, Canada

JAMES R. DRUMMOND

Department of Physics, University of Toronto, Toronto, Ontario, Canada, and Department of Physics and Atmospheric Science, Dalhousie University, Halifax, Nova Scotia, Canada

PIERRE F. FOGAL

Department of Physics, University of Toronto, Toronto, Ontario, Canada

(Manuscript received 2 September 2008, in final form 16 January 2009)

ABSTRACT

A new Bruker IFS 125HR Fourier transform spectrometer has been installed at the Polar Environment Atmospheric Research Laboratory at Eureka, Nunavut, Canada (80.05°N, 86.42°W). This instrument will become the Network for the Detection of Atmospheric Composition Change's (NDACC's) primary instrument at Eureka, replacing the existing Bomem DA8 Fourier transform spectrometer, and will operate throughout the sunlit parts of the year. This paper introduces the new instrument and describes the retrieval procedure, including a comprehensive error analysis. Total columns of O_3, HCl, HF, HNO_3, N_2O, CH_4, and CO are presented for the first full year of measurements (2007). Perturbations in the total column resulting from the presence of the Arctic polar vortex over Eureka and the chemical processes within it are visible, as are annual cycles driven by photochemistry and dynamics. Enhancements in the CO total column resulting from specific biomass burning smoke events can also be seen. An intercomparison between the existing Bomem DA8 and the new Bruker IFS 125HR was carried out in July 2007 and is presented here. The total columns derived from the two instruments are shown to be in excellent agreement, with mean differences for all gases of less than 2.3%.

1. Introduction

Ground-based Fourier transform infrared (FTIR) spectrometers are routinely used around the globe for the measurement of atmospheric trace gases by solar absorption spectroscopy. The high spectral resolution of these instruments, combined with the large number of trace gases that have absorption features in the infrared, make the FTIR spectrometer uniquely capable of providing simultaneous column measurements of multiple gases from the ground. By utilizing height information contained in the pressure broadening of the absorption features, FTIR spectra can also be used to provide some information about the vertical distribution profiles of many of these gases (Pougatchev et al. 1995; De Mazière et al. 2005; Schneider et al. 2008).

The Network for the Detection of Atmospheric Composition Change (NDACC; information online at http://www.ndacc.org) consists of a network of well-characterized instruments, including FTIR spectrometers, in locations from the Arctic to the Antarctic. In addition to providing

Corresponding author address: Rebecca Batchelor, Dept. of Physics, University of Toronto, 60 St. George St., Toronto, ON M5S 1A7, Canada.
E-mail: rbatchelor@atmosp.physics.utoronto.ca

DOI: 10.1175/2009JTECHA1215.1

time series of trace gas information that in many cases stretches back decades (e.g., the Kitt Peak, Lauder, and Jungfraujoch time series), thus allowing the determination of trends (Rinsland et al. 1998, 2003; Zander et al. 2008; Vigouroux et al. 2008), NDACC FTIR instruments are frequently used for the validation of satellite measurements (e.g., Dils et al. 2006; Strong et al. 2008; Kerzenmacher et al. 2008).

The Polar Environment Atmospheric Research Laboratory (PEARL, formerly the Arctic Stratospheric Ozone, or AStrO, Observatory) at Eureka, Nunavut, Canada (80.05°N, 86.42°W, 610 m ASL) is part of the Arctic primary NDACC site, and has had an ABB Bomem DA8 FTIR spectrometer, operated by Environment Canada and the Meteorological Research Institute of Japan, since 1993 (Donovan et al. 1997; Kerzenmacher et al. 2005; Farahani et al. 2007). As part of the recent rejuvenation of the PEARL laboratory by the Canadian Network for the Detection of Atmospheric Change (CANDAC), a new Bruker IFS 125HR FTIR spectrometer was installed at PEARL in July 2006. This instrument is a very high spectral resolution commercial spectrometer that is able to operate semi-autonomously throughout the sunlit parts of the Arctic year. After receiving its NDACC certification, the 125HR fully replaced the ABB Bomem DA8 as the PEARL primary instrument following the DA8's removal in February 2009. This paper serves as an introduction for the new PEARL FTIR spectrometer, which will be described in detail in section 2. Analysis details, error analysis, and data from its first full year of operation will be presented in sections 3, 4, and 5, respectively. Finally, the results of a summertime intercomparison exercise between the new and existing instruments will be presented in section 6, with the goal of ensuring that the consistency and high quality of FTIR data from Eureka are maintained.

2. The PEARL Bruker IFS 125HR

The PEARL Bruker IFS 125HR (henceforth referred to as the 125HR) is a scanning Michelson interferometer with corner-cube retroreflectors, optimized for solar absorption spectroscopy in the infrared. It gives high quality spectra at a resolution of up to 0.0024 cm^{-1} (where resolution is defined as 0.9/maximum optical path difference, and the maximum optical path difference for the 125HR is 372 cm). The beamsplitter is permanently aligned at 30° incidence, with a repeatable locking mount that allows easy exchange and automatic recognition of either of its two beamsplitters: the potassium chloride (KBr) beamsplitter for mid-infrared measurements from 450 to 4800 cm^{-1}, and the calcium fluoride (CaF_2) beamsplitter for near-infrared measurements from 1200 to 15 000 cm^{-1}. A helium neon laser is used for precise location of the scanning mirror, which uses a dc motor and a linear drive unit for smooth gliding along its track. Interferograms are recorded on either of two liquid-nitrogen-cooled detectors: the photovoltaic indium antimonide (InSb) or photoconductive mercury–cadmium–telluride (MCT) detectors. These detectors are sensitive to radiation from 1850 to 10 000 cm^{-1} (5–1 μm) and 600 to 6000 cm^{-1} (16–1.6 μm), respectively, and are typically used in conjunction with one of eight standard NDACC narrow-bandpass filters (listed in Table 1), which limit the wavenumber range of the spectra, thus increasing the signal-to-noise ratio. The whole system is operated under vacuum, with a scroll pump used to maintain the pressure at less than 1 hPa.

TABLE 1. NDACC narrow-band filters used in the 125HR.

Filter No.	Wavenumber range (cm^{-1})
1	3950–4300
2	2700–3500
3	2420–3080
4	1950–2700
5	1800–2200
6	700–1350
7	700–1000
8	1000–1400

Sunlight comes from the existing custom-built active solar tracker located on the roof of PEARL. Flat mirrors inside the laboratory direct the beam to either the existing Bomem DA8 or to the 125HR using a kinematic mount for reproducibility. In addition to the solar source, the 125HR has two internal sources for the mid- and near-infrared regions. Approximately every 2 months, an NDACC cell containing a known amount of HBr gas (Coffey et al. 1998) is placed in the sample compartment, and spectra are recorded using the internal mid-infrared source. These spectra are used to determine the instrument line shape using the LINEFIT 9.0 code, as described by Hase et al. (1999). To date, the instrument has maintained near-perfect alignment, with the modulation efficiency along its path in excess of 98%. The phase error is less than 0.035 rad, with a peak at approximately 50 cm.

Routine direct-sun absorption measurements are made whenever possible during the sunlit parts of the polar year (approximately 21 February–20 October). Measurements are only possible when clouds are very thin or the sky is clear. In standard operation, the 125HR measures through each of its filters in turn, utilizing a macro to adjust the preamplifier gain to maximize the signal (though note that filter 7 was only installed in August 2007, and filter 8 is not in routine

use). Four scans at 0.0035 cm^{-1} resolution (corresponding to a maximum optical path difference is 250 cm), recorded in both the forward and backward scanning directions and taking approximately 6 min, are recorded and coadded for each spectrum. In addition to routine measurements, the 125HR has been used in five campaigns, during which measurements were tailored to meet the goals of the campaigns. These campaigns have included (i) the 2007 and 2008 Canadian Arctic Atmospheric Chemistry Experiment (ACE) Validation Campaigns, when the 125HR was operated in conjunction with the Bomem DA8 and the University of Waterloo Portable Atmospheric Research Interferometric Spectrometer for the Infrared (PARIS-IR); (ii) an intensive 125HR–Bomem DA8 intercomparison exercise in July 2007, as described in section 6; (iii) an NDACC National Aeronautics and Space Administration (NASA) *Aura* satellite validation campaign in August–September 2007, when coordinated measurements tailored to match the gases of interest were made at NDACC FTIR sites around the globe; and (iv) measurements during an aircraft overflight that was part of the NASA Arctic Research of the Composition of the Troposphere from Aircraft and Satellites (ARCTAS; information online at http://www.espo.nasa.gov/arctas) mission in April 2008, when the instrument was operated in the near-infrared in support of the Total Carbon Column Observing Network (TCCON) effort (Washenfelder et al. 2006).

3. Data analysis

Spectra have been analyzed using SFIT2 version 3.92c (Pougatchev et al. 1995; Hase et al. 2004) and the High-Resolution Transmission Molecular Absorption Database (HITRAN) 2004 + updates spectroscopic line list (Rothman et al. 2005). SFIT2 is a radiative transfer and profile retrieval algorithm based on the optimal estimation technique of Rodgers (1976, 1990, 2000), whereby a calculated spectrum is fitted to the observed one by means of adjustment of the gas profile and supplementary instrumental parameters. The forward model is a multilayer, multispecies line-by-line radiative transfer model utilizing a Voigt line shape function (Pougatchev et al. 1995), with refractive ray-tracing and mass path calculations performed using the FASTCODE (or FSCATM) algorithm (Meier et al. 2004; Wood et al. 2004) and site-specific pressure and temperature information. SFIT2 is widely used by the FTIR community (e.g., Pougatchev et al. 1995; Rinsland et al. 1998; Wood et al. 2004; Senten et al. 2008) and has recently undergone an extensive validation exercise (Hase et al. 2004).

While FTIR spectra and SFIT2 can be used for the retrieval of more than 20 different trace gas columns, for the purposes of this paper, we have concentrated on several key NDACC species—O_3, HCl, HNO_3, and HF—as representative of predominantly stratospheric trace gases and CH_4, N_2O, and CO as representative of predominantly tropospheric species. Additional species have been retrieved but are not described here.

The 125HR retrievals have been performed using a 38-layer retrieval grid that increases by approximately 4% in thickness for each successive layer, from 0.8-km thickness at 1 km to 13 km at 100 km, with a higher-resolution 63-layer grid used for the ray-tracing calculation. A priori volume mixing ratio (VMR) profiles developed for the Eureka site (K. Sung et al., unpublished manuscript) have been used for all retrievals except CO, which uses data from the Mk-IV balloon-borne instrument (Toon et al. 1999) launched from Kiruna, Sweden (67.8°N, 20.4°E). A priori covariances have been fixed at constant values consistent with the maximum variability derived from satellite data (K. Sung et al., unpublished manuscript), with interlayer correlations also derived from satellite data applied to the a priori covariances for HCl, HF, and O_3. Temperature and pressure information has been derived from the mean of the radiosondes that are launched twice daily at 1100 and 2300 UTC at Eureka, spliced to the daily National Centers for Environmental Protection (NCEP) profiles above the balloon maximum heights (these are calculated directly for NDACC sites and available online at ftp://ftp.cpc.ncep.noaa.gov/ndacc/ncep), and then to the *U.S. Standard Atmosphere, 1976* profile above 50 km (National Aeronautics and Space Administration 1976). The microwindows (small regions of the spectra containing the absorption lines of interest) used for the retrievals have been selected from a range of sources (De Mazière et al. 2004; Fu et al. 2008; K. Sung et al., unpublished manuscript) based on the spectral regions of the 125HR and DA8 filters, spectroscopic errors, and the information content in the retrievals. With recent improvements in computer processing, retrievals over large microwindows or simultaneously over multiple microwindows have become possible, leading to improved retrievals (Barret et al. 2002; De Mazière et al. 2004; Schneider and Hase, 2008). This ability has been exploited for many of the gases. Table 2 lists the microwindows used for retrieving the gases described in this paper. Also given are the interfering species in each window (which are typically fitted with a simple scaling of the corresponding a priori VMR profile), the a priori covariance and correlation length (applied as a Gaussian, with the correlation length specifying the half-width), and the degrees of freedom of signal (DOFS, explained below). Instrument line shape parameters, background slope and curvature, wavelength and

TABLE 2. Summary of the retrieval parameters used for 125HR fits. Multiple microwindows listed for a single gas are fitted simultaneously. Interfering species are scale fitted. Here, σ indicates the square root of the diagonal elements of the a priori covariance matrix, $\mathbf{S}_a$, with the half-width half-maximum value of the interlayer correlation length applied to that matrix given as Corr. The ad hoc SNR and typical values of the DOFS are also given.

Gas	Microwindow(s) (cm^{-1})	Interfering species (scale fitted only)	σ (%)	Corr (km)	SNR	DOFS
O_3	1000.0–1004.5	H_2O, CO_2, $O_3$676, $O_3$667, $O_3$686, $O_3$668, C_2H_4	70	4	100	~7
HCl	2775.72–2775.8	O_3, CH_4, N_2O	50	5	100	~2.5
	2821.4–2821.62	HDO, N_2O				
	2925.75–2926.05	CH_4, NO_2, OCS, O_3				
HF	4038.78–4039.1	H_2O, CH_4, HDO	50	5	100	~2
HNO_3	867.5–870.0	H_2O, OCS, NH_3	100	0	100	~2
N_2O	2481.3–2482.6	H_2O, HDO, CO_2, O_3, CH_4	50	0	70	~4
	2526.4–2528.2	H_2O, HDO, CO_2, O_3, CH_4				
	2537.85–2538.8	H_2O, HDO, CO_2, O_3, CH_4				
	2540.1–2540.7	H_2O, HDO, CO_2, O_3, CH_4				
CH_4	2613.7–2615.4	HDO, N_2O, CO_2	50	0	70	~3.5
	2650.6–2651.3	HDO, N_2O, CO_2				
	2835.5–2935.8	HDO, N_2O, CO_2				
	2903.6–2904.03	HDO, N_2O, CO_2				
	2921.0–2921.6	HDO, N_2O, CO_2				
CO	2057.68–2058.0	O_3, CO_2, OCS	20	0	200	~2.7
	2069.56–2069.76	O_3, CO_2, OCS				
	2157.507–2159.144	O_3, N_2O, H_2O				

zero-level shift parameters, and a simple phase error parameter have also been retrieved.

While the signal-to-noise ratios (SNRs) of the actual spectra are very high (sometimes over 1000), the ad hoc SNR is a fitting parameter [which defines the measurement noise covariance $\mathbf{S}_\varepsilon$ with diagonal elements set to $1/(\mathrm{SNR})^2$ and is used as a weighting parameter against the a priori covariance $\mathbf{S}_a$] that has been tuned to ensure optimal fitting of the calculated to the measured spectra. This is done by plotting the ''trade-off curve'' of the root-mean-square (RMS) fitting residual against SNR for each gas. The use of low values of SNR results in high RMS residuals when insufficient information is being taken from the measurement. As the SNR is increased, the RMS residual decreases as the measurement contributes to the retrieval, then levels off, at which point the retrieval is attempting to fit noise. An ad hoc value of SNR near the elbow of this trade-off curve thus ensures that the measurements are not being overfitted. Values of SNR between 70 and 200 as listed in Table 2 have been used for these retrievals, with one value used consistently for all spectra of a given gas. Higher SNR values tend to cause unrealistic oscillations in the retrieved profiles, in agreement with the trade-off curve suggestion of overfitting. Examples of the spectral fits and the associated residuals obtained for one of the microwindows for each of the gases are shown in Fig. 1. Note that these have been taken from midsummer spectra (7 August 2007). The appearance of the fits can change significantly through the year, with much deeper absorption lines (and correspondingly higher SNRs) resulting from the sun's long path through the atmosphere near polar sunrise and sunset, and shallower lines when the sun is high in the sky in midsummer.

While SFIT2 is a profile retrieval algorithm, and the optimal fit for the observed spectra has been determined by adjustment of the profile on a 38-layer retrieval grid, ground-based FTIR spectra do not contain sufficient information for 38 independent pieces of information, and thus the retrieved profile should be treated with caution. The DOFS, in this case defined as the trace of the averaging kernel matrix (Rodgers 2000), provides an estimate of the number of independent pieces of information in the measurement. Utilizing the DOFS and the averaging kernels, partial columns covering height ranges of interest can be determined from the retrieved profiles. Examples of total and partial column-averaging kernels for each of the gases are shown in Fig. 2. The number of DOFSs in the total column is given in Table 2.

4. Error analysis

An estimate of the uncertainty in the measurements has been made following the methodology of Rodgers (1990, 2000) and is shown in Table 3. In addition to smoothing error ($\mathbf{S}_s$, also referred to as the null-space error) and measurement error ($\mathbf{S}_m$) as described in those references, the error in the retrieved column due to other retrieved parameters, termed interference errors, have been calculated as described in Rodgers

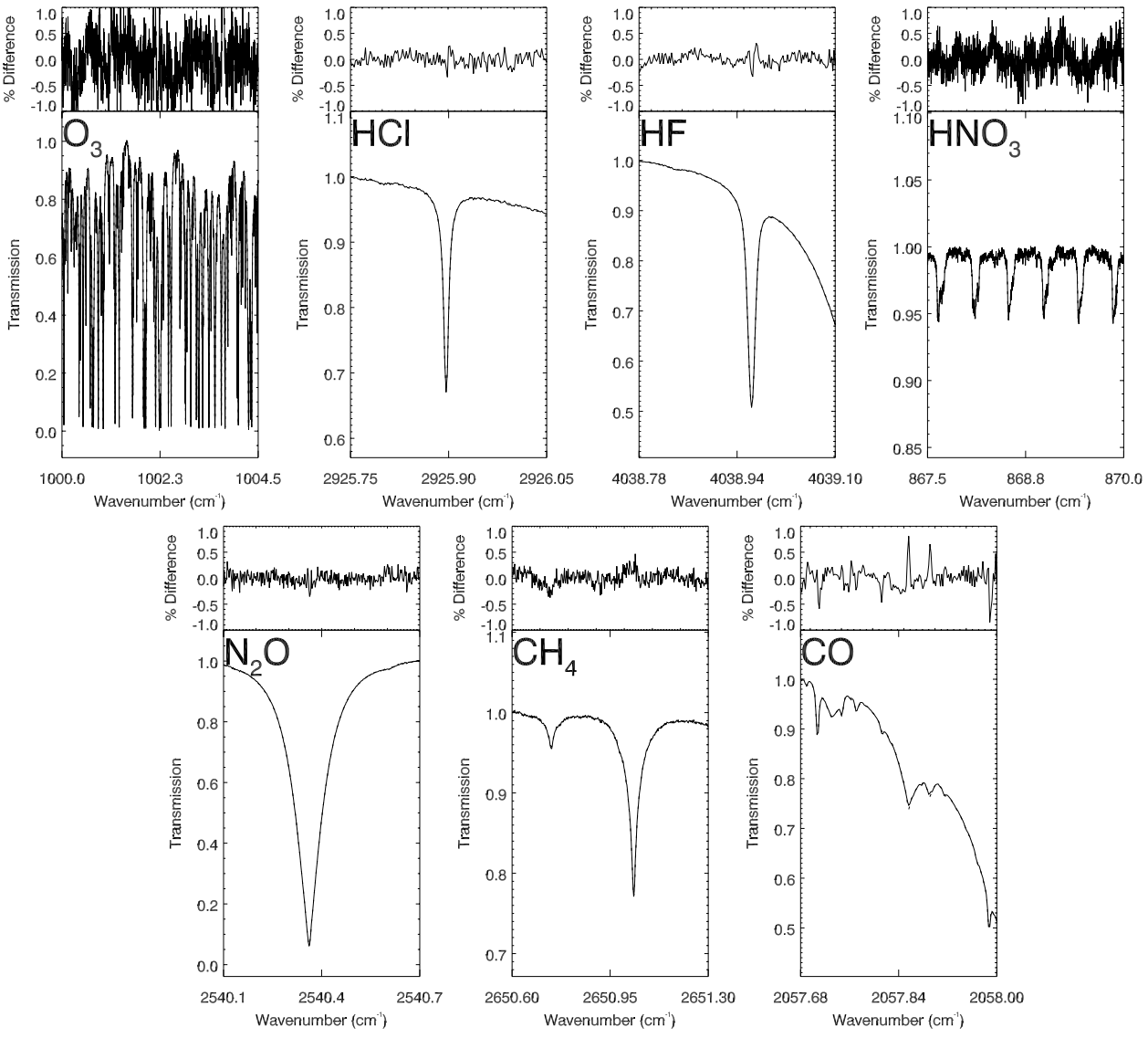

FIG. 1. Example fits and residuals for one microwindow from each of O_3, HCl, HF, HNO_3, N_2O, CH_4, and CO. All examples are from spectra recorded on 7 Aug 2007 with the 125HR. Measured spectra are shown by the gray solid line, and calculated spectra are shown by the dashed black line. Residuals are determined from the difference between the measured and calculated spectra.

and Connor (2003). In this case, the interference errors include errors due to interfering species and due to retrieval parameters such as wavelength shift, instrument line shape, background slope and curvature, zero-level shift, and phase error. In Table 3, the interference errors have been broken into two components: those caused by interfering species ($\mathbf{S}_{\text{int\_spec}}$) and those caused by retrieval parameters ($\mathbf{S}_{\text{int\_ret}}$). In addition, forward model parameter errors (generically, $\mathbf{S}_f$) have been determined using Eq. (3.18) in Rodgers (2000), reproduced as

$$\mathbf{S}_f = \mathbf{G}_y \mathbf{K}_b \mathbf{S}_b \mathbf{K}_b^{\mathrm{T}} \mathbf{G}_y^{\mathrm{T}}, \tag{1}$$

where $\mathbf{G}_y$ is the gain matrix, or the sensitivity of the retrieval with respect to the measurement; $\mathbf{K}_b$ is the sensitivity of the forward model with respect to the model parameter, determined empirically using a small perturbation of the parameter; and $\mathbf{S}_b$ is described by our best estimate of the uncertainty in that parameter. For the error resulting from uncertainty in solar zenith angle ($\mathbf{S}_{\text{sza}}$), an $\mathbf{S}_b$ of 0.125° was used, corresponding to the maximum change in solar zenith angle from the center point where the solar zenith angle was calculated to the end of a 6-min measurement. Note that in most cases, the solar zenith angle changes by substantially less than this amount. Likewise, uncertainties

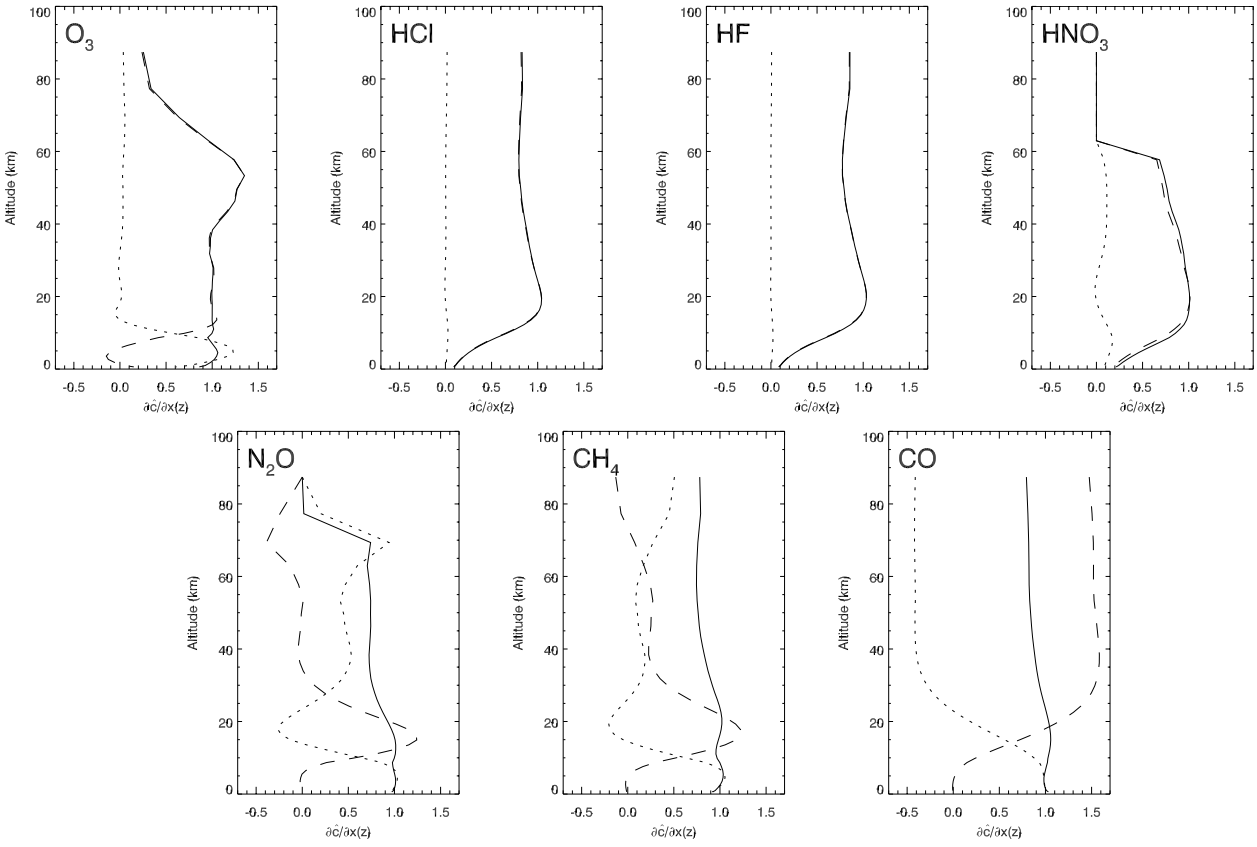

FIG. 2. Typical averaging kernels for O_3, HCl, HF, HNO_3, N_2O, CH_4, and CO retrievals, as determined from spectra recorded on 7 Aug 2007. Solid lines show the total column averaging kernel. Dotted lines show the 0–10-km partial column, representative of the troposphere, and dashed lines show the 10–50-km partial column, representative of the stratosphere.

resulting from line parameters have been determined by perturbing each of the line intensities ($\mathbf{S}_{\text{lineint}}$) and the air-broadened half-widths ($\mathbf{S}_{\text{airbroad}}$) for all lines of the species of interest. In this case, $\mathbf{S}_b$ has been determined from the maximum uncertainty within the range quoted in the HITRAN 2004 line list (Rothman et al. 2005). In the cases where the uncertainty in the line parameters was unknown (HNO_3 and O_3 line intensity), a conservative estimate of 20% was used. Finally, forward model errors associated with the temperature profile ($\mathbf{S}_{\text{temp}}$) have been estimated by perturbing the temperature in each layer in turn. The $\mathbf{S}_b$ matrix in this case was determined from the uncertainties quoted in the NCEP profiles, specifically 2 K below 30 km, 5 K between 30 and 35 km, 6 K between 35 and 40 km, 7 K from 40 to 50 km, and 9 K above. An 8-km correlation length was also applied, making this $\mathbf{S}_b$ nondiagonal.

In interpreting the errors listed in Table 3, it is worth noting that a clear division between systematic and random uncertainties is not straightforward. While the

TABLE 3. Summary of the error budgets (%) for the total columns (0.61–100 km) for each trace gas. Errors are determined from the square roots of the indicated covariance matrices, which are defined in section 3. These estimates are appropriate for July, when the sun is highest and the absorption lines are shallow. When the sun is lower, the error estimates decrease in all cases.

Gas	$\mathbf{S}_S$ (%)	$\mathbf{S}_m$ (%)	$\mathbf{S}_{\text{int\_spec}}$ (%)	$\mathbf{S}_{\text{int\_ret}}$ (%)	$\mathbf{S}_{\text{sza}}$ (%)	$\mathbf{S}_{\text{lineint}}$ (%)	$\mathbf{S}_{\text{airbroad}}$ (%)	$\mathbf{S}_{\text{temp}}$ (%)	$\mathbf{S}_{\text{TOT}}$ (%)
O_3	0.3	0.2	0.0	0.0	0.2	10.5	0.5	0.8	10.5
HCl	1.3	2.1	0.5	2.0	0.4	1.6	0.8	0.6	3.7
HF	1.1	1.8	0.2	1.0	0.4	4.0	0.1	0.9	4.7
HNO_3	1.9	3.0	2.3	0.2	0.3	15.6	2.2	1.1	16.4
N_2O	0.2	0.3	0.1	0.3	0.3	3.8	0.7	0.1	3.9
CH_4	0.8	1.1	0.2	1.1	0.4	16.5	2.6	0.6	16.8
CO	0.1	0.3	0.0	0.1	0.1	1.5	1.3	0.2	2.1

uncertainty due to measurement noise ($\mathbf{S}_m$) is considered to be truly random, and the uncertainty due to spectroscopic parameters ($\mathbf{S}_{\text{lineint}}$ and $\mathbf{S}_{\text{airbroad}}$) is mostly systematic, other uncertainty sources, including the estimate of the smoothing effect of the retrieval on the true profile ($\mathbf{S}_s$), uncertainty due to the retrieved interfering species and line shape parameters ($\mathbf{S}_{\text{int\_ret}}$ and $\mathbf{S}_{\text{int\_spec}}$), errors due to changes in the solar zenith angle through the measurement ($\mathbf{S}_{\text{sza}}$), and errors in the temperature profile ($\mathbf{S}_{\text{temp}}$), vary on different time scales, from spectra to spectra, day to day, or season to season. As such, the total error ($\mathbf{S}_{\text{TOT}}$) listed in Table 3 has been determined by adding all errors in quadrature as suggested by the International Organization for Standardization (1993), with no separation of systematic and random effects. Note that in many cases, the smoothing error ($\mathbf{S}_s$) can be removed when performing a comparison by smoothing a higher-resolution measurement with the averaging kernel and a priori of the lower-resolution measurement (Rodgers and Connor 2003), and that spectroscopic errors can be discounted when looking for trends or specific events in the 125HR data itself (they contribute to the accuracy of the retrieved columns, rather than the precision). The error bars in the graphs presented in section 5 include all error sources.

5. Results from the first full year of 125HR data

While measurements were first made during August and September 2006, and are currently on going, 2007 encompasses the first full year of 125HR spectra, from sunrise in late February until sunset in late October. The total columns derived from those measurements are presented here. PEARL, at 80.05°N and remote from local emissions, is an interesting site for measurements in both the spring period, when the polar vortex is frequently overhead and thus conditions are driven by vortex dynamics and ozone depletion chemistry, and the summer, when perturbations of trace gas concentrations result from the transport of pollutants from lower latitudes. Photochemistry also plays an important role in the observed trends, as day length increases from 24-h darkness in February to 24-h daylight by early April, and reverts from 24-h daylight to 24-h darkness between late August and mid-October. Figure 3 shows the total columns of each of our gases of interest along with the total errors, as determined for each individual measurement. Note that the larger error bars for HNO_3 and CH_4 are primarily due to the spectroscopic uncertainties in HITRAN 2004, as seen in Table 3. The data gap for all gases in April resulted from operational constraints, while the gap in the gases retrieved on the MCT detector (O_3 and HNO_3) in June was caused by removal of the detector for a minor fix.

There are several features of note in Fig. 3. There is a large perturbation, particularly visible in the stratospheric gases, from approximately days 65 to 85. The 2006/07 Arctic polar winter was characterized by a strong cold polar vortex that lasted well into the spring, with significant ozone depletion recorded within it (Rösevall et al. 2007). The 125HR measurements from PEARL sampled the air inside the vortex from approximately day 65 to day 85 and, as such, measurements from those days are characteristic of the chemically processed and dynamically isolated air within the vortex. This is being investigated in greater detail in a paper currently in preparation.

Outside of this period, we see that the total columns of HCl and HF—the primary reservoirs of inorganic chlorine and fluorine, respectively—remain relatively constant, with short-term fluctuations reflected in both gases. As these gases are both generally unreactive in the nonvortex stratosphere, they can be regarded as tracers of stratospheric dynamics, and the small variations as indications of the different air masses that are being sampled. These fluctuations are also visible to a lesser degree in the O_3 and HNO_3 results. In addition to these fluctuations, in the O_3 data, the annual cycle driven by the Brewer–Dobson circulation can be seen, with a maximum in late winter/early spring and a minimum in summer. The photolytic processes that convert odd nitrogen (NO and NO_2) into HNO_3 during periods of darkness, and back during daylight, can also be seen in the decreasing columns of HNO_3 as the year progresses into summer, and increasing columns as it moves back toward the polar night.

The N_2O and CH_4 total columns both contain a stratospheric contribution of about 20%. The influence of this contribution is visible as a perturbation in the total column resulting from the polar vortex. This is much less obvious for CO, which has a very small stratospheric contribution to the total column. Aside from the small variation resulting from the polar vortex, CH_4 columns remain effectively constant throughout the year, while CO columns demonstrate a strong seasonal cycle resulting from the annual cycle of OH. This is supplemented by anthropogenic emissions of CO from industry and biomass burning in Europe and Siberia, which are transported into the Arctic atmosphere and, in the absence of sunlight and OH, accumulate over the polar winter (Novelli et al. 1998; Zhao et al. 2002; Stohl et al. 2007). With a lifetime of weeks to months in the atmosphere, during which time it may be transported many hundreds of kilometers from its source of origin, CO is a well-known biomass burning

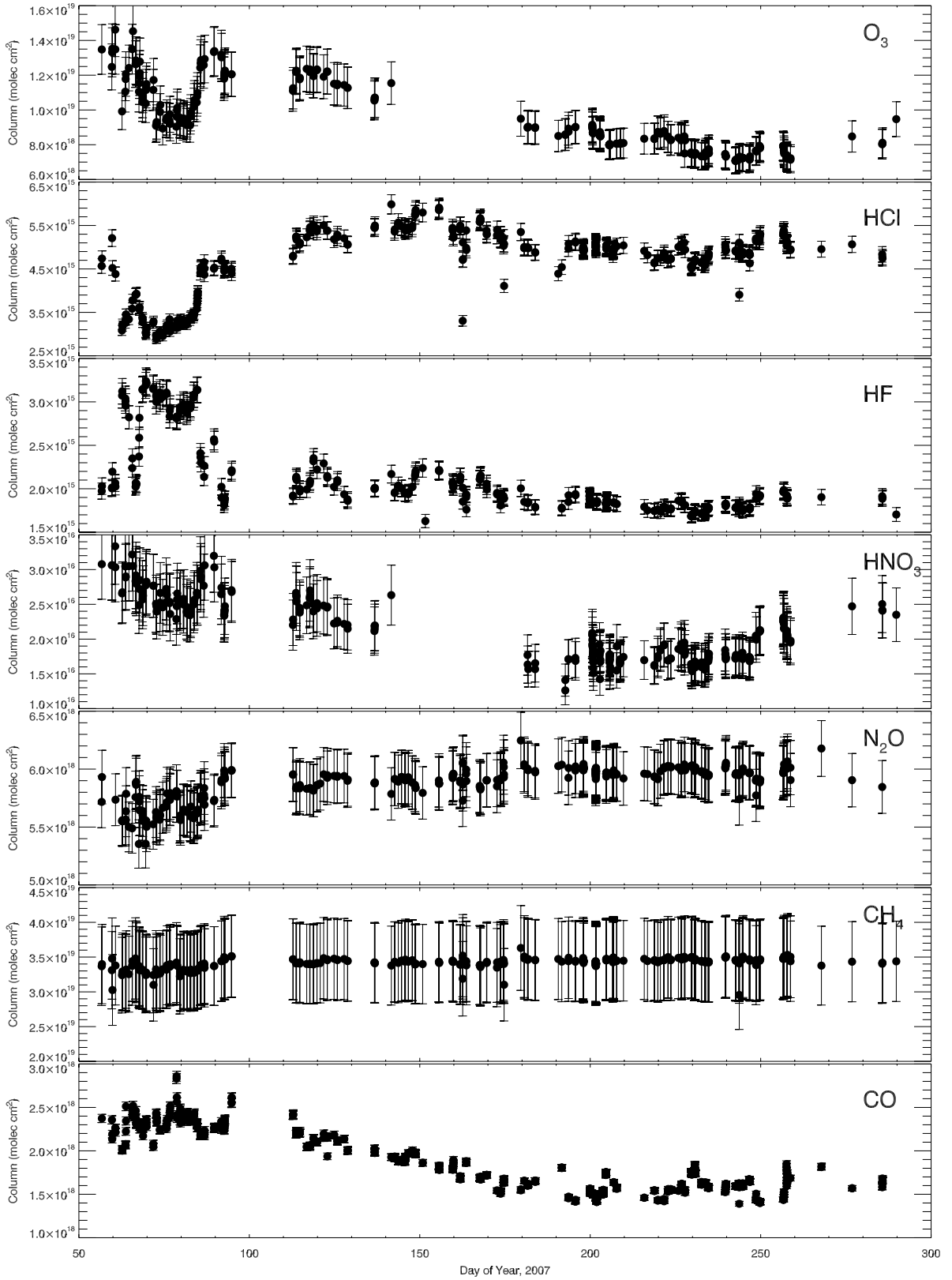

FIG. 3. Total columns of O_3, HCl, HF, HNO_3, N_2O, CH_4, and CO, by day of year during 2007. Each point represents an individual measurement. Error bars indicate the total error, as given in Table 3.

indicator and tracer of smoke pollution (Rinsland et al. 1998; Zhao et al. 2002). Outlying maxima in the CO column, for example on days 192, 205–207, and 230–231, can be traced to specific smoke events, as shown in O'Neill et al. (2008).

Also clear from Fig. 3 is the internal consistency of the 125HR data. There is little scatter from day to day, and trends and interesting events stand out clearly. The 125HR measurements made during the July intercomparison exercise, when atmospheric conditions were very stable, showed a typical standard error about the mean of less than 1% throughout the day, as will be shown in section 6.

6. Bruker 125HR–Bomem DA8 instrument intercomparison

From 15 to 25 July 2007, the 125HR and the existing Eureka Bomem DA8 underwent a comprehensive 2-week intercomparison exercise, in preparation for exchanging the old primary NDACC FTIR instrument for a new one. During July, atmospheric conditions are fairly stable, with little transport of air from the midlatitudes and no significant diurnal cycle (due to 24-h sunlight). As such, little variation is expected in these trace gases through the course of the day. In addition, we experienced very clear skies, making this an ideal time for an intercomparison.

a. The Environment Canada Bomem DA8

The Environment Canada ABB Bomem DA8 FTIR spectrometer (henceforth the DA8) was installed at PEARL (then known as the AStrO Observatory) in 1993, and has been operated during each polar sunrise and most polar sunset periods since that time (Farahani et al. 2007). It is a vertically aligned high-resolution spectrometer capable of making single-sided scans at up to 0.0035 cm^{-1} resolution (250-cm maximum optical path difference), with a series of eight narrow-bandpass filters. It is not operated under vacuum, but at room pressure. A KBr beamsplitter is used with two liquid-nitrogen-cooled detectors (InSb and MCT) similar to those of the 125HR. Typically, DA8 measurements consist of four coadded scans, Fourier transformed with a Hamming apodization function applied to the interferograms to reduce interference from the sidelobes caused by truncation of the interferograms at the end of a scan. The DA8 has participated in five Canadian Arctic ACE Validation campaigns (Kerzenmacher et al. 2005; Fu et al. 2008; K. Sung et al., unpublished manuscript); has been used for lunar (Farahani et al. 2007), NO (Wiacek et al. 2006), and ClO (Donovan et al. 1997) measurements; and has undergone a validation exercise with the National Physical Laboratory's traveling Bruker 120M (Paton-Walsh et al. 2008). In the latter, the mean agreement between the two instruments during the April–May 1999 validation campaign was around 3% for all species (HCl, CH_4, N_2O, O_3, CO_2, N_2, HNO_3) except HF, for which the agreement was approximately 7% (Paton-Walsh et al. 2008). A comparison of partial columns derived from the DA8 and the Atmospheric Chemistry Experiment Fourier Transform Spectrometer (ACE-FTS; Bernath et al. 2005) by Fu et al. (2008) showed mean differences for O_3, HNO_3, HF, and HCl ranging from 0.9% for HF to 8.5% for HCl (Fu et al. 2008). This is consistent with the differences relative to ACE-FTS partial columns found using other NDACC ground-based FTIR spectrometers (Dupuy et al. 2008; Mahieu et al. 2008; Wolff et al. 2008).

b. Intercomparison methodology

For this campaign, specialized measurements were obtained specifically for the purpose of the intercomparison. A single solar tracker was used, with the light beam being directed alternately into the 125HR, then to the DA8, then back to the 125HR. To gain suitable statistics, it was decided that a set of approximately 16 measurements should be made with each instrument, with each filter, on any given day. In the interests of time, rather than recording four-scan coadds, single scans were recorded for each of the InSb filters. The single-scan SNR, however, was too low for the DA8 MCT detector and filter 6 (700–1300 cm^{-1}); therefore, for this filter, four scans were coadded on both instruments. Single-scan measurements each took approximately 1.5 min, although the time required for the DA8 to Fourier transform the interferogram prior to the next measurement was as much as 12 min, depending on the size of the spectrum. Thus, in general, the time between a DA8 and a 125HR measurement was approximately 3 min, and the time between successive DA8 measurements ranged from 3 to 12 min. Additional 125HR spectra were recorded while the DA8 was processing. Weather conditions throughout the campaign were near perfect, with continuous clear skies on most days. Measurements were made through very thin cirrus for short periods on days 197, 199, and 204.

Trace gas profiles were retrieved from the spectra of both instruments using SFIT2, though in the case of the DA8, this was SFIT2 version 3.91 (the differences from this to version 3.92c being minor, mostly coding or isotopic changes for gases not used in these retrievals). An identical HITRAN 2004 + updates spectroscopic line list was used for both sets of retrievals, as described previously. A priori profiles, a priori covariances, pressure and temperature profiles, and retrieval parameters

were also identical between the instruments, and were consistent with those described in section 3.

c. Results

Total columns of each of the seven gases of interest were determined from the retrieved profiles and the air masses determined by the forward model. For each day, a mean total column was determined for each of the instruments, and the difference for that day was calculated as follows:

$$\Delta TC = \frac{(\overline{TC}_{125HR} - \overline{TC}_{DA8})}{0.5(\overline{TC}_{125HR} + \overline{TC}_{DA8})}, \quad (2)$$

where $\overline{TC}_{125HR}$ is the 125HR daily mean total column and $\overline{TC}_{DA8}$ is the DA8 daily mean total column.

Table 4 shows the daily mean total column ($\overline{TC}$), the standard deviation (SD), and the standard error on the mean (SE = SD/$\sqrt{N}$, where N is the number of measurements on the day) for each day, for each instrument. The daily mean difference between the 125HR and DA8 columns and the combined SD and SE are also shown.

d. Discussion of results

From Table 4, we can see that in nearly all cases, the 125HR and the DA8 agree within their combined standard deviations, and that the general agreement between the two instruments is excellent and is, in fact, significantly better than would have been expected based on the previous intercomparison between this DA8 and the National Physical Laboratories traveling Bruker 120M in Eureka in 1999 (Paton-Walsh et al. 2008). As mentioned previously, the earlier comparison showed the mean of the daily mean differences (or campaign mean, calculated over 3 days in that comparison) to be around 3% for all gases except HF, for which the difference was around 7%. In the current comparison, the campaign mean (calculated over 2–4 days) of the differences is even lower—less than 1.7% (and generally less than 1%) for all gases except O_3, for which there was a slightly higher campaign mean difference of 2.3%.

There are several factors that we believe contribute to this improvement, in addition to the change of comparison instrument. First, these total columns are obtained using a profile retrieval algorithm (SFIT2) instead of a simpler profile-scaling algorithm (SFIT). This allows the retrieval to cope much better with an a priori profile that is not perfectly shaped than in the previous study. In addition, we have performed most of these retrievals over multiple microwindows. This provides the retrieval with more information than in the case of a single microwindow. Additional instrument parameters, including the zero-level shift, which was identified as a source of error in the earlier comparison (Paton-Walsh et al. 2008), are now fitted routinely within SFIT2, thus eliminating some of the problems of the earlier campaign and allowing small errors in the instrument line shape to be corrected. Finally, we have used updated line parameters, in the form of HITRAN 2004 + updates, as opposed to HITRAN 1996. While the line parameters do provide a generally systematic bias, any particularly erroneous parameters can have undesired effects on the retrieval and leave significant residuals in the fits.

From Table 4, we are also able to see that the scatter on a given day, as evidenced by the standard deviation, is significantly less for the new 125HR than for the older DA8. While this is to be expected from a new, modern instrument, it is a reassuring assessment of the quality of the 125HR data. The standard error for the 125HR, which provides an estimate of the random measurement noise (as well as any variability in the gas through the day) is very low and is consistent with (or less than) the estimated error due to measurement noise shown in Table 3.

In addition to the previous Eureka intercomparison, there have been a series of other NDACC intercomparison exercises around the world (Walsh et al. 1997; Goldman et al. 1999; Griffith et al. 2003; Meier et al. 2005). These have typically shown agreement between NDACC-quality instruments, compared side by side, of 1%–2% for tropospheric gases, and 2%–3% for stratospheric gases. As the results of this comparison are well within these levels of agreement, we are confident that the 125HR is an NDACC-quality instrument, and that changing from the DA8 as the primary Eureka FTIR to the 125HR will cause no discontinuities or step functions in the Eureka long-term data record when the spectra are analyzed in a consistent manner. Thus, the high quality of the Eureka dataset will be maintained.

7. Conclusions

A new Bruker 125HR Fourier transform spectrometer has been installed at PEARL, Eureka, Nunavut (80.05°N, 86.42°W), Canada, for the measurement of atmospheric trace gases in the mid-infrared. This paper has described the new instrument, the retrieval process being used to analyze the data, and the error analysis. Total columns of O_3, HCl, HF, HNO_3, N_2O, CH_4, and CO from 2007, the first full year of 125HR operation, have been presented. The perturbed conditions that result from the Arctic polar vortex are clearly visible during the spring period in the gases found predominantly in the stratosphere. In all of the gases, the annual cycle observed is consistent with our current understanding of

TABLE 4. Results from the 125HR–DA8 summer intercomparison exercise at PEARL. Values apply to the 125HR, DA8, or Combined 125HR and DA8. Datasets use the same terminology as detailed in Eq. (2). Here, $\overline{TC}$ indicates the daily mean total column amount, N is the number of measurements, SD is the standard deviation, and SE is the standard error on the mean ($SD/N^{0.5}$). The column difference, ΔTC, has been determined as defined in Eq. (2). The combined SD and SE have been determined by adding the individual SD and SE, respectively, for the two instruments in quadrature.

		125HR				DA8				Combined		
Gas	Day	$\overline{TC}_{125HR}$ (mol cm^{-2})	N	SD (%)	SE (%)	$\overline{TC}_{DA8}$ (mol cm^{-2})	N	SD (%)	SE (%)	ΔTC (%)	SD (%)	SE (%)
O_3	200	8.80×10^{18}	19	1.94	0.45	9.01×10^{18}	17	2.79	0.68	2.36	3.40	0.81
	202	8.58×10^{18}	19	0.82	0.19	8.74×10^{18}	16	1.33	0.33	1.85	1.56	0.38
	205	8.00×10^{18}	19	0.22	0.05	8.21×10^{18}	16	1.27	0.32	2.59	1.29	0.32
									Mean	2.27		
HCl	197	4.94×10^{15}	33	0.57	0.10	4.86×10^{15}	12	6.11	1.76	1.64	6.14	1.77
	201	5.04×10^{15}	45	0.85	0.13	5.18×10^{15}	16	3.18	0.79	−2.65	3.29	0.80
	204	5.00×10^{15}	17	0.45	0.11	4.80×10^{15}	16	8.44	2.11	4.08	8.45	2.11
	206	4.92×10^{15}	22	0.61	0.13	4.85×10^{15}	20	4.06	0.91	1.53	4.11	0.92
									Mean	1.15		
HF	199	1.89×10^{15}	22	0.89	0.19	1.88×10^{15}	17	1.80	0.44	0.35	2.01	0.48
	201	1.85×10^{15}	17	0.43	0.10	1.80×10^{15}	16	2.49	0.62	2.42	2.52	0.63
	204	1.85×10^{15}	63	0.75	0.09	1.81×10^{15}	16	3.33	0.83	2.20	3.42	0.84
									Mean	1.65		
HNO_3	200	1.82×10^{16}	18	8.24	1.94	1.88×10^{16}	17	9.46	2.29	−3.45	12.54	3.01
	202	1.76×10^{16}	11	7.42	2.24	1.79×10^{16}	16	9.13	2.28	−1.30	11.76	3.20
	205	1.69×10^{16}	13	5.04	1.40	1.63×10^{16}	16	3.38	0.84	3.38	6.06	1.63
									Mean	−0.46		
N_2O	197	6.01×10^{18}	33	0.20	0.03	5.86×10^{18}	12	2.56	0.74	2.43	2.57	0.74
	201	5.97×10^{18}	45	0.36	0.05	6.02×10^{18}	16	1.97	0.49	−0.77	2.00	0.49
	206	5.96×10^{18}	10	0.14	0.04	5.98×10^{18}	10	0.77	0.24	−0.27	0.79	0.25
									Mean	0.47		
CH_4	197	3.44×10^{19}	33	0.37	0.06	3.39×10^{19}	12	3.37	0.97	1.47	3.39	0.97
	201	3.41×10^{19}	45	0.47	0.07	3.43×10^{19}	16	2.19	0.55	−0.66	2.24	0.55
	206	3.46×10^{19}	10	0.57	0.18	3.42×10^{19}	10	1.55	0.49	1.03	1.65	0.52
									Mean	0.61		
CO	201	1.46×10^{18}	44	0.44	0.07	1.47×10^{18}	17	2.34	0.57	−1.04	2.38	0.57
	203	1.53×10^{18}	46	1.04	0.15	1.53×10^{18}	16	1.93	0.48	−0.27	2.20	0.51
									Mean	−0.65		

atmospheric chemistry and dynamics. Specific enhancements from individual smoke events are also visible in the CO total column results.

The 125HR has now replaced the existing Bomem DA8 as the NDACC FTIR instrument at Eureka. To confirm the consistency of the data, an instrument intercomparison was completed in July 2007 and is presented here. Mean differences in the total column between the 125HR and the DA8 were less than 2.3% for all gases, and less than 1% for each of the tropospheric gases. These values are well within the differences found during other NDACC intercomparisons. As such, we are confident that when the data are analyzed in a consistent manner, there will be no major discrepancies in the Eureka dataset as one instrument replaces the other and that the high quality of data from PEARL will be maintained into the future.

Acknowledgments. We gratefully acknowledge the support of the CANDAC operators Ashley Harrett, Alexei Khmel, Paul Loewen, Oleg Mikhailov, and Matt Okraszewski for collecting 125HR data for us when we were not on site, and the Environment Canada weather station for their hospitality when we were. We also acknowledge Tony Eng, Gregor Surawicz, and Keith MacQuarrie for their assistance in installing the 125HR. In addition, we are grateful to Environment Canada for providing radiosonde data. Logistical and on-site support in Eureka was provided by CANDAC. CANDAC and PEARL are funded by the Atlantic Innovation Fund/Nova Scotia Research Innovation Trust, Canadian Foundation for Climate and Atmospheric Sciences, Canadian Foundation for Innovation, Canadian Space Agency, Environment Canada, Government of Canada International Polar Year funding, Natural Sciences and Engineering Research Council, Ontario Innovation Trust, Polar Continental Shelf Program, and the Ontario Research Fund. The Canadian Arctic ACE Validation Campaigns are co-led by Kaley Walker of the University of Toronto and supported by the Canadian

Space Agency, Environment Canada, NSERC, and the Northern Scientific Training Program.

REFERENCES

Barret, B., M. De Mazière, and P. Demoulin, 2002: Retrieval and characterization of ozone profiles from solar infrared spectra at the Jungfraujoch. *J. Geophys. Res.,* **107,** 4788, doi:10.1029/2001JD001298.

Bernath, P. F., and Coauthors, 2005: Atmospheric Chemistry Experiment (ACE): Mission overview. *Geophys. Res. Lett.,* **32,** L15S01, doi:10.1029/2005GL022386.

Coffey, M. T., A. Goldman, J. W. Hannigan, W. G. Mankin, W. G. Schoenfeld, C. P. Rinsland, C. Bernardo, and D. W. T. Griffith, 1998: Improved vibration-rotation (0-1) HBr line parameters for validating high resolution infrared atmospheric spectra measurements. *J. Quant. Spectrosc. Radiat. Transfer,* **60,** 863–867.

De Mazière, M., and Coauthors, 2004: Ground-based FTIR measurements of O3- and climate-related gases in the free troposphere and lower stratosphere. *Proc. Quadrennial Ozone Symp.,* Kos, Greece, International Association for Meteorology and Atmospheric Sciences/International Ozone Commission, 529–530.

——, and Coauthors, 2005: The exploitation of ground-based Fourier transform infrared observations for the evaluation of tropospheric trends of greenhouse gases over Europe. *Environ. Sci. J. Integr. Environ. Res.,* **2,** 283–293.

Dils, B., and Coauthors, 2006: Comparisons between SCIAMACHY and ground-based FTIR data for total columns of CO, CH_4, CO_2 and N_2O. *Atmos. Chem. Phys.,* **6,** 1953–1976.

Donovan, D. P., and Coauthors, 1997: Ozone, column ClO, and PSC measurements made at the NDSC Eureka Observatory (80°N, 86°W) during the spring of 1997. *Geophys. Res. Lett.,* **24,** 2709–2712.

Dupuy, E., and Coauthors, 2008: Validation of ozone measurements from the Atmospheric Chemistry Experiment (ACE). *Atmos. Chem. Phys. Discuss.,* **8,** 2513–2656.

Farahani, E. E., and Coauthors, 2007: Nitric acid measurements at Eureka obtained in winter 2001–2002 using solar and lunar Fourier transform absorption spectroscopy: Comparisons with observations at Thule and Kiruna and with results from three-dimensional models. *J. Geophys. Res.,* **112,** D01305, doi:10.1029/2006JD00709605.

Fu, D., and Coauthors, 2008: Simultaneous atmospheric measurements using two Fourier transform infrared spectrometers at the Polar Environment Atmospheric Research Laboratory during spring 2006, and comparisons with the Atmospheric Chemistry Experiment-Fourier Transform Spectrometer. *Atmos. Chem. Phys. Discuss.,* **8,** 5305–5358.

Goldman, A., and Coauthors, 1999: Network for the detection of stratospheric change Fourier transform infrared intercomparison at Table Mountain Facility, November 1996. *J. Geophys. Res.,* **104,** 30 481–30 503.

Griffith, D. W. T., N. B. Jones, B. McNamara, C. P. Walsh, W. Bell, and C. Bernardo, 2003: Intercomparison of NDSC ground-based solar FTIR measurements of atmospheric gases at Lauder, New Zealand. *J. Atmos. Oceanic Technol.,* **20,** 1138–1153.

Hase, F., T. Blumenstock, and C. Paton-Walsh, 1999: Analysis of the instrumental line shape of high-resolution Fourier transform IR spectrometers with gas cell measurements and new retrieval software. *Appl. Opt.,* **38,** 3417–3422.

——, J. W. Hannigan, M. T. Coffey, A. Goldman, M. Höpfner, N. B. Jones, C. P. Rinsland, and S. W. Wood, 2004: Intercomparison of retrieval codes used for the analysis of high-resolution, ground-based FTIR measurements. *J. Quant. Spectrosc. Radiat. Transfer,* **87,** 25–52.

International Organization for Standardization, 1993: *Guide to the Expression of Uncertainty in Measurement*. 1st ed, 101 pp.

Kerzenmacher, T. E., and Coauthors, 2005: Measurements of O_3, NO_2 and temperature during the 2004 Canadian Arctic ACE validation campaign. *Geophys. Res. Lett.,* **32,** L16S07, doi:10.1029/2005GL023032.

——, and Coauthors, 2008: Validation of NO_2 and NO from the Atmospheric Chemistry Experiment (ACE). *Atmos. Chem. Phys.,* **8,** 3529–3562.

Mahieu, E., and Coauthors, 2008: Validation of ACE-FTS v2.2 measurements of HCl, HF, CCl_3F and CCl_2F_2 using space-, balloon- and ground-based instrument observations. *Atmos. Chem. Phys. Discuss.,* **8,** 3431–3495.

Meier, A., A. Goldman, P. S. Manning, T. M. Stephen, C. P. Rinsland, N. B. Jones, and S. W. Wood, 2004: Improvements to air mass calculations for ground-based infrared measurements. *J. Quant. Spectrosc. Radiat. Transfer,* **83,** 109–113.

——, and Coauthors, 2005: Evidence of reduced measurement uncertainties from an FTIR instrument intercomparison at Kiruna, Sweden. *J. Quant. Spectrosc. Radiat. Transfer,* **96,** 75–84.

National Aeronautics and Space Administration, 1976: *U.S. Standard Atmosphere*. U.S. Government Printing Office, Washington, DC, 241 pp.

Novelli, P. C., K. A. Masarie, and P. M. Lang, 1998: Distributions and recent changes of carbon monoxide in the lower troposphere. *J. Geophys. Res.,* **103,** 19 015–19 033.

O'Neill, N. T., and Coauthors, 2008: Occurrence of weak, submicron, tropospheric aerosol events at high Arctic latitudes. *Geophys. Res. Lett.,* **35,** L14814, doi:10.1029/2008GL033733.

Paton-Walsh, C., R. L. Mittermeier, W. Bell, H. Fast, N. Jones, and A. Meier, 2008: An intercomparison of ground-based solar FTIR measurements of atmospheric gases at Eureka, Canada. *J. Atmos. Oceanic Technol.,* **25,** 2028–2036.

Pougatchev, N. S., B. J. Connor, and C. P. Rinsland, 1995: Infrared measurements of the ozone vertical distribution above Kitt Peak. *J. Geophys. Res.,* **100** (D8), 16 689–16 697.

Rinsland, C. P., and Coauthors, 1998: Northern and Southern Hemisphere ground-based infrared spectroscopic measurements of tropospheric carbon monoxide and ethane. *J. Geophys. Res.,* **103,** 28 197–28 217.

——, and Coauthors, 2003: Long-term trends of inorganic chlorine from ground-based infrared solar spectra: Past increases and evidence for stabilization. *J. Geophys. Res.,* **108,** 4252, doi:10.1029/2002JD003001.

Rodgers, C. D., 1976: Retrieval of atmospheric temperature and composition from remote measurements of thermal radiation. *Rev. Geophys. Space Phys.,* **14,** 609–624.

——, 1990: Characterization and error analysis of profiles retrieved from remote sounding measurements. *J. Geophys. Res.,* **95** (D5), 5587–5595.

——, 2000: *Inverse Methods for Atmospheric Sounding: Theory and Practice*, World Scientific, 238 pp.

——, and B. J. Connor, 2003: Intercomparison of remote sounding instruments. *J. Geophys. Res.,* **108,** 4116, doi:10.1029/2002JD002299.

Rösevall, J. D., D. P. Murtagh, and J. Urban, 2007: Ozone depletion in the 2006/2007 Arctic winter. *Geophys. Res. Lett.,* **34,** L21809, doi:10.1029/2007GL030620.

Rothman, L. S., and Coauthors, 2005: The HITRAN 2004 molecular spectroscopic database. *J. Quant. Spectrosc. Radiat. Transfer,* **96,** 139–204.

Schneider, M., and F. Hase, 2008: Recipe for monitoring of total ozone with a precision of around 1 DU applying mid-infrared solar absorption spectra. *Atmos. Chem. Phys.,* **8,** 63–71.

——, ——, T. Blumenstock, A. Redondas, and E. Cuevas, 2008: Quality assessment of O_3 profiles measured by a state-of-the-art ground-based FTIR observing system. *Atmos. Chem. Phys. Discuss.,* **8,** 4977–5006.

Senten, C., and Coauthors, 2008: New ground-based FTIR measurements at Ile de La Réunion: Observations, error analysis, and comparisons with independent data. *Atmos. Chem. Phys.,* **8,** 3483–3508.

Stohl, A., and Coauthors, 2007: Arctic smoke—Record high air pollution levels in the European Arctic due to agricultural fires in eastern Europe in spring 2006. *Atmos. Chem. Phys.,* **7,** 511–534.

Strong, K., and Coauthors, 2008: Validation of ACE-FTS N_2O measurements. *Atmos. Chem. Phys.,* **8,** 4759–4786.

Toon, G. C., and Coauthors, 1999: Comparison of MkIV balloon and ER-2 aircraft measurements of atmospheric trace gases. *J. Geophys. Res.,* **104,** 26 779–26 790.

Vigouroux, C., and Coauthors, 2008: Evaluation of tropospheric and stratospheric ozone trends over western Europe from ground-based FTIR network observations. *Atmos. Chem. Phys. Discuss.,* **8,** 5007–5059.

Walsh, C. P., and Coauthors, 1997: An uncertainty budget for ground-based Fourier transform infrared column measurements of HCl, HF, N_2O, and HNO_3 deduced from results of side-by-side instrument intercomparisons. *J. Geophys. Res.,* **102,** 8867–8873.

Washenfelder, R. A., and Coauthors, 2006: Carbon dioxide column abundances at the Wisconsin Tall Tower site. *J. Geophys. Res.,* **111,** D22305, doi:10.1029/2006JD007154.

Wiacek, A., N. B. Jones, K. Strong, J. R. Taylor, R. L. Mittermeier, and H. Fast, 2006: First detection of meso-thermospheric nitric oxide (NO) by ground-based FTIR solar absorption spectroscopy. *Geophys. Res. Lett.,* **33,** L03811, doi:10.1029/2005GL024897.

Wolff, M. A., and Coauthors, 2008: Validation of HNO_3, $ClONO_2$, and N_2O_5 from the Atmospheric Chemistry Experiment Fourier Transform Spectrometer (ACE-FTS). *Atmos. Chem. Phys.,* **8,** 3529–3562.

Wood, S. W., and Coauthors, 2004: Ground-based nitric acid measurements at Arrival Heights, Antarctica, using solar and lunar Fourier transform infrared observations. *J. Geophys. Res.,* **109,** D18307, doi:10.1029/2004JD004665.

Zander, R., and Coauthors, 2008: Our changing atmosphere: Evidence based on long-term infrared solar observations at the Jungfraujoch since 1950. *Sci. Total Environ.,* **391,** 184–195.

Zhao, Y., and Coauthors, 2002: Spectroscopic measurements of tropospheric CO, C_2H_6, C_2H_2, and HCN in northern Japan. *J. Geophys. Res.,* **107,** 4343, doi:10.1029/2001JD000748.